



HAL
open science

Generalized phonon density of states of Mo₃Sb₇ and Mo₃Sb_{5.4}Te_{1.6} from inelastic neutron scattering and lattice dynamical calculations.

Christophe Candolfi, Bertrand Lenoir, Anne Dauscher, Michael Marek Koza, Marc de Boissieu, Malgorzata Sternik, Krzysztof Parlinski

► To cite this version:

Christophe Candolfi, Bertrand Lenoir, Anne Dauscher, Michael Marek Koza, Marc de Boissieu, et al.. Generalized phonon density of states of Mo₃Sb₇ and Mo₃Sb_{5.4}Te_{1.6} from inelastic neutron scattering and lattice dynamical calculations.. Physical Review B: Condensed Matter and Materials Physics (1998-2015), 2011, 84 (22), 10.1103/PhysRevB.84.224306 . hal-00664704

HAL Id: hal-00664704

<https://hal.science/hal-00664704>

Submitted on 23 Feb 2023

HAL is a multi-disciplinary open access archive for the deposit and dissemination of scientific research documents, whether they are published or not. The documents may come from teaching and research institutions in France or abroad, or from public or private research centers.

L'archive ouverte pluridisciplinaire **HAL**, est destinée au dépôt et à la diffusion de documents scientifiques de niveau recherche, publiés ou non, émanant des établissements d'enseignement et de recherche français ou étrangers, des laboratoires publics ou privés.

Generalized phonon density of states of Mo_3Sb_7 and $\text{Mo}_3\text{Sb}_{5.4}\text{Te}_{1.6}$ from inelastic neutron scattering and lattice dynamical calculations

C. Candolfi ^{*†}, B. Lenoir, A. Dauscher

Institut Jean Lamour (UMR 7198 CNRS - Nancy-Université - UPV - Metz)

Ecole Nationale Supérieure des Mines de Nancy - Parc de Saurupt, 54042 Nancy cedex

M. M. Koza

Institut Laue-Langevin, 6 rue Jules Horowitz, BP 156, F-38042 Grenoble Cedex 9, France

M. de Boissieu

Laboratoire de Science et Ingénierie des Matériaux et Procédés (SIMaP), Grenoble-INP,

UJF, CNRS, BP 75, 38402 Saint-Martin-d'Hères Cedex, France

M. Sternik, K. Parlinski

Institute of Nuclear Physics, Polish Academy of Science, Radzikowskiego 152, PL-31342

Cracow, Poland

* Corresponding author: christophe.candolfi@cpfs.mpg.de

† Present address: Max-Planck-Institut für Chemische Physik fester Stoffe, Nöthnitzer Str. 40, 01187 Dresden, Germany.

PACS number: 78.70.Nx, 63.20.-e

Abstract

The temperature dependence of the generalized phonon density of states (GDOS) of polycrystalline Mo_3Sb_7 and $\text{Mo}_3\text{Sb}_{5.4}\text{Te}_{1.6}$ was studied from 300 down to 2 K using inelastic neutron scattering. Even though Mo_3Sb_7 undergoes a magnetic as well as a structural phase transition at $T^* = 53$ K, no appreciable change in the recorded spectra has been revealed. The generalized density of states of the non-magnetic $\text{Mo}_3\text{Sb}_{5.4}\text{Te}_{1.6}$ compound shows similar main characteristics though substituting Sb by Te leads to a shift of the entire spectrum towards higher energy. The temperature dependence of the GDOS reveals an anomalous softening of phonons with decreasing temperature in Mo_3Sb_7 which cannot be captured by the harmonic approximation while $\text{Mo}_3\text{Sb}_{5.4}\text{Te}_{1.6}$ exhibits a normal behaviour. This feature might be related to a strong interplay between magnetic excitations and phonons at the core of the anomalous thermal transport displayed by Mo_3Sb_7 . In general, the main characteristics of the experimentally derived GDOS of Mo_3Sb_7 can be reproduced by lattice dynamical calculations.

I. Introduction

Inelastic neutron scattering (INS) constitutes a powerful tool to probe elementary excitations in magnetic and non-magnetic solids. INS experiments enable to investigate in detail the lattice dynamics of crystalline materials, the superconducting order parameter of unconventional superconductors as well as to obtain a deeper insight into the symmetries and driving forces of magnetic ground states.¹⁻⁴

The Mo_3Sb_7 compound has recently attracted attention due to the coexistence of type-II superconductivity below $T_c \sim 2.3$ K and low dimensional magnetism related to

antiferromagnetically coupled molybdenum dimers that lead to the formation of a spin gap below $T^* = 53$ K.^{5,6} Several studies with the aim at determining the symmetry of the order parameter of the superconducting state have been undertaken. While specific heat analysis as well as muon spin spectroscopy measurements have suggested a single isotropic energy gap,^{7,8} further experimental investigations using muon spin relaxation appeared to be consistent with the existence of two superconducting BCS-like gaps, even though these results are still under debate.⁹⁻¹¹ In addition, Wiendlocha et al.¹² have successfully estimated the experimental electron-phonon coupling constant from combined first-principle electronic band structure and lattice dynamical calculations.

The formation of the spin gap in Mo_3Sb_7 is accompanied by a structural transition breaking the cubic symmetry of the crystalline lattice.^{13,14} Uncommon temperature dependences of the transport properties, i.e. of the electrical resistivity, thermopower and thermal conductivity were reported. These investigations have provided insights into the coupling between the different degrees of freedom of the system i.e. between phonons, electrons and magnetic dimers.¹⁵ In this regard, strong interactions of phonons with localized magnetic dimers have been suggested as the prominent scattering mechanism controlling the thermal transport.¹⁵ Further experimental evidence of this interplay was provided by detailed studies of the transport properties of the ternary $\text{Mo}_3\text{Sb}_{7-x}\text{Te}_x$ and $\text{Mo}_{3-x}\text{Ru}_x\text{Sb}_7$ systems.¹⁶⁻¹⁹ Diluting the magnetic interactions by increasing the Te and Ru contents was then found to progressively restore a conventional temperature dependence of the thermal conductivity.

Recently, muon spin relaxation combined with inelastic neutron scattering experiments performed on the Mo_3Sb_7 and Ru_3Sn_7 compounds were reported further confirming the formation of a spin gap in Mo_3Sb_7 .²⁰ In this context, a thorough investigation and analysis of the lattice dynamics of this compound may provide additional information to help understand the anomalous thermal transport of the binary compound and on its behaviour upon alloying.

Here we report inelastic neutron scattering measurements of the generalized density of states (GDOS) of Mo_3Sb_7 and of the non-magnetic and isostructural $\text{Mo}_3\text{Sb}_{5.4}\text{Te}_{1.6}$ compound in the 2 – 300 K temperature range. These experimental results are confronted with a phonon density of states (PDOS) and temperature dependence of the specific heat of Mo_3Sb_7 derived by lattice dynamical calculations and discussed in light of the aforementioned unconventional behaviour of the thermal conductivity.

II. Experimental detail

Polycrystalline Mo_3Sb_7 and $\text{Mo}_3\text{Sb}_{5.4}\text{Te}_{1.6}$ samples have been prepared by reaction of stoichiometric amounts of high purity Mo powders (99.999%), Sb and Te shots (99.999%) in quartz ampoules sealed under an inert atmosphere (He- H_2 , 95-5%). The ampoules were then heated up to 750°C and kept at this temperature for 10 days. The obtained ingots were ground and further annealed at the same temperature for 15 days to ensure a good chemical homogeneity. X-ray and neutron powder-diffraction studies have been performed on both samples and have shown that Mo_3Sb_7 contained a negligible amount (< 2% vol.) of antimony as a secondary phase while $\text{Mo}_3\text{Sb}_{5.4}\text{Te}_{1.6}$ did not exhibit any secondary phases.²¹ These results were further corroborated by electron probe microanalysis. The Table I summarizes the lattice parameters of both compounds together with the data on the low-temperature phase of Mo_3Sb_7 inferred from X-ray powder diffraction.

To determine the GDOS, $G(\omega)$, INS experiments were carried out at room temperature on the high resolution time-of-flight spectrometer IN6 and extended down to 2 K using the thermal time-of-flight spectrometer IN4 of the European neutron source, Institut Laue-Langevin in Grenoble, France. IN6 experiments were performed on ~ 10 g of powdered Mo_3Sb_7 and $\text{Mo}_3\text{Sb}_{5.4}\text{Te}_{1.6}$ placed in a cylindrical aluminum can with a radius of 4 mm

resulting in a transmission of $\sim 89\%$. Data were recorded at 300 K with an incident neutron wavelength of 4.14 Å in the inelastic time-focusing mode to attain a high energy resolution ($\sim 200 - 400 \mu\text{eV}$ in the 0 – 20 meV energy range).²² An elastic Q range of up to the (4.0.0) zone center has been covered with this setup. Since the IN6 spectrometer exploits the anti-Stokes line of scattering processes, this setup enabled us to probe the low temperature inelastic response of the compounds down to ~ 100 K in the entire energy range of vibrational excitations. To access lower temperatures, IN4 experiments were carried out on ~ 40 g of Mo_3Sb_7 and $\text{Mo}_3\text{Sb}_{5.4}\text{Te}_{1.6}$ powders. A flat, thin-walled aluminum sample holder was utilized resulting in a sample layer thickness of 6 mm. The transmission of the samples was $\sim 90\%$. Data on both compounds were recorded in the neutron-energy-loss mode (Stokes side) at 220, 100, 70, 50 and 2 K using two distinct incident neutron wavelengths of 1.22 and 1.80 Å. A maximum elastic Q range of up to the (8.8.8) and (14.0.0) zone centers have been covered with the 1.22 Å setup.

Standard data corrections for empty container scattering and detector calibration using an incoherent standard (vanadium) have been applied. Using the incoherent approximation that implies an averaging of the inelastic signal over the accessed momentum space, the data were converted into the generalized density of states $G(\omega)$ applying established mathematical relations.²³⁻²⁶ All $G(\omega)$ presented in this paper are normalized to 30 phonon modes in the 0.5-36 meV energy range for both spectrometers.

An estimation of a potential multiphonon contribution by a self-consistent technique indicates the presence of an additional weak background in the recorded spectra. We assume that a minute amount of hydrogen as a remnant of the sample preparation is present in our samples. Note that in terms of scattering power (see Table IV) a single hydrogen atom scatters more than 10^3 times more neutrons than any of the sample constituents. It is worth mentioning that this contribution neither affects our analysis nor our conclusions.

Lattice dynamical calculations were carried out using the Vienna Ab-Initio Simulation Package (VASP) and the direct phonon method within the software package PHONON. Some data are discussed in detail elsewhere.^{12,27} In the present paper, total PDOS together with the temperature dependence of the specific heat, C_V , calculated within the framework of harmonic solids, are presented.

III. Results

A. Generalized density of states $G(\omega)$

Figure 1 reports the GDOS of Mo_3Sb_7 and $\text{Mo}_3\text{Sb}_{5.4}\text{Te}_{1.6}$ measured at 300 K with the IN6 spectrometer. Both data sets show an intensity cutoff at ~ 36 meV limiting the $G(\omega)$ to this energy range. Referring to the lattice dynamical calculation results (see Ref. 12 and below), the intensity in the energy region $\hbar\omega < 20$ meV can be associated with modes strongly weighted by Sb motion whereas the higher energy part of $G(\omega)$ is weighted by Mo amplitudes. Note that the crystalline structure is characterized by one Mo site and two distinct Sb sites, denoted hereafter as Sb1 and Sb2 leading to the extended chemical formula $\text{Mo}_3(\text{Sb1})_3(\text{Sb2})_4$. Beyond this rough graduation of $G(\omega)$ distinct peaks may be identified. The main peaks were fitted with gaussian functions and were found to be centered at $\hbar\omega \approx 8.4, 14.8, 18.5$ and 27.7 meV and $9.2, 14.4, 20.4$ and 29.8 meV for Mo_3Sb_7 and $\text{Mo}_3\text{Sb}_{5.4}\text{Te}_{1.6}$, respectively. From these phonon spectra, a rough estimation of the Debye temperature θ_D can

be inferred from the relation $\theta_D = \frac{4}{3} \frac{\langle E \rangle}{k_B}$ where k_B is the Boltzmann constant and

$\langle E \rangle = \int \omega G(\omega) d\omega$ is the first moment of energy.²⁸ With $\langle E \rangle = 16.4$ and 17.6 meV for

Mo₃Sb₇ and Mo₃Sb_{5.4}Te_{1.6}, respectively, we then obtain respective θ_D of 255 and 272 K. These values are in fair agreement with those derived from low temperature specific heat analyses on both samples, and neutron diffraction experiments along with ultrasound velocity measurements for Mo₃Sb₇ (Table II).^{7,16,29}

The careful reader might notice that the low energy region tends to deviate from a harmonic Debye behavior for which $G(\omega) \propto \omega^2$. As shown in Figure 2, this feature is due to a dispersive band coming from acoustic phonons which originate from a Bragg reflection located above the highest 2θ angle that could be attained in the present experiment. In other words, the incoherent approximation is not fully fulfilled for the intensity distribution at the lowest energies and high Q values in the IN6 data. However, the prominent peaks at higher energies are not affected by this deviation as they originate from rather localized, non-dispersive modes (i.e. modes for which the group velocity vanishes $\partial\omega/\partial Q \sim 0$) detectable in a vast region of the phase space.

The PDOS $Z(\omega)$ of Mo₃Sb₇ derived from lattice dynamical calculations has been previously published in Ref. 12. In this paper, the simulated PDOS displays one phonon peak close to 4 meV. This low-energy excitation does not show up in the measured density of states, shown in Figure 1. This low energy mode originates in the simulation from a longitudinal excitation which becomes soft at the high symmetry point H. Using similar Hellmann-Feynman forces as those used in Ref. 12, we have introduced a dispersion of the previously flat phonon curve originating from a longitudinal acoustic branch as seen in Figure 3. To derive these dispersion curves, it was sufficient to change only six diagonal independent force-constant parameters of the Mo-Mo and Sb-Sb pairs by unexpected small magnitudes of 0.17% and 0.70%, respectively, all calculated with respect to the xx component of the Mo-Mo on-side force constant (Table III). The remaining 344 independent force-constant parameters remained practically unchanged (within numerical noise which was less than 0.005 %).

Intriguing is the fact that so small changes of the force-constant parameters are able to renormalize the phonon to distinctly higher energies.¹²

Using these new force constants, we have calculated the total and partial PDOS shown in Figure 4a. Note that in order to allow for a direct comparison with experiments, $Z(\omega)$ has been convolved with a gaussian function whose width approximates the energy resolution of the instrument.²² A good agreement between the simulation and our measurements can be observed.

Even though Sb and Te display similar atomic radii, molar masses and total scattering power (Table IV), modifications arise from the substitution of Sb by Te (Figure 1). A prominent effect of the substitution on the inelastic response is the shift of the full phonon spectrum towards higher energies. This observation is qualitatively in agreement with the unit cell contraction as the Te concentration increases.^{16,21}

Beyond the overall shift of $G(\omega)$, the distribution of the modes is not preserved by the partial substitution of Sb by Te. As Figure 1 shows, the presence of Te influences some distinct eigenmodes. It has been shown from powder neutron diffraction experiments together with electronic band structure calculations that Te is exclusively located on the Sb1 site.²¹ As shown in Figure 4b which depicts the partial density of states of Mo and Sb, the Sb1 and Sb2 sites display different $Z(\omega)$ contributions. It is thus likely that this partial substitution may only influence some distinct phonon modes resulting in slight differences between the two spectra.

Based upon the lattice dynamical calculations, the specific heat $C_V(T)$ of Mo_3Sb_7 has been computed and compared with experimental data $C_p(T)$ in Figure 5a, whereby we assume the difference $C_p - C_V = \alpha^2 BVT$, where α is the volumic thermal expansion coefficient, B the bulk modulus, V the specific volume and T the absolute temperature, to be negligible.³⁰ An overall satisfactory match between computed and measured data can be

observed. The slight discrepancy above 150 K is likely related to the anharmonicity of the crystalline lattice which is not captured by the calculations. Below the characteristic temperature T^* , the position of the peak in the C_p/T^3 data is well reproduced by the calculations. The more pronounced discrepancy between the two sets of data (Figure 5b) may raise the question whether or not the cubic-to-tetragonal distortion of the crystal structure (see Table I)^{13,14} can be held responsible of this difference.

On a more quantitative level, the lattice contribution to the specific heat $C_{V,ph}(T)$ can be inferred from the experimental INS data via the relation

$$C_{V,ph}(T) = 3k_B \int_0^\infty G(\omega) \left(\frac{\hbar\omega}{k_B T} \right)^2 \frac{\exp\left[\frac{\hbar\omega}{k_B T} \right]}{\left(\exp\left[\frac{\hbar\omega}{k_B T} \right] - 1 \right)^2} d\omega \quad (1)$$

As shown in Figures 6a and 6b, the INS data reproduce well the temperature dependence of the experimental $C_p(T)$ for both compounds. Note that in the case of the Te-substituted sample, the somewhat stronger discrepancy between the two sets of data towards room temperature may be due to a higher experimental uncertainty in the measurement of the C_p values above ~ 250 K. Prior investigations have revealed that the magnetic properties of the binary compound lead to a substantial contribution to the specific heat at low temperatures which progressively disappears with increasing the Te content.^{6,16} The $C_p(T)$ data of Mo_3Sb_7 can be thus decomposed into three terms

$$C_p(T) = C_{lattice}(T) + C_e(T) + C_{mag}(T) = C_{V,ph}(T) + \gamma T + \frac{(\Delta/k_B T)^2 \exp(\Delta/k_B T)}{[1 + 3 \exp(\Delta/k_B T)]^2} \quad (2)$$

where $C_e(T) = \gamma T$ is the electronic contribution with γ the Sommerfeld coefficient and

$C_{mag}(T) = \frac{(\Delta/k_B T)^2 \exp(\Delta/k_B T)}{[1 + 3 \exp(\Delta/k_B T)]^2}$ is the magnetic contribution originating from the

antiferromagnetically-coupled Mo dimers in which Δ is the width of the spin gap which opens below T^* . In Eq.(2), we make the reasonable assumption that the anharmonic contribution within the quasiharmonic approximation is negligible in the temperature range investigated i.e. $C_{lattice}(T) = C_{V,ph}(T)$. Tran et al. have shown that the magnetic contribution can be described by a spin gap model of isolated dimers.⁶ In the present case, $C_{mag}(T)$ can be determined by subtracting the lattice and electronic contributions from the experimental $C_p(T)$ data. As a first approximation, we have assumed the γ parameter to be temperature-independent ($\gamma \sim 34.5 \text{ mJ.mol}^{-1}.\text{K}^{-2}$ [11,16]). The temperature dependence of $C_{mag}(T)$ obtained by this approach (see Figure 6a) is in good agreement with that derived by Tran et al.⁶ using an isostructural and non-magnetic compound as a phonon reference. In the Te-substituted sample, the subtraction of the lattice contribution leads to the temperature dependence of the electronic contribution $C_e(T)$. As can be seen in Figure 6b, no significant magnetic contribution can be identified in agreement with the low-temperature transport property and magnetic susceptibility data indicating a strong weakening of the magnetic interactions upon alloying on the Sb or the Mo sites.^{16,18}

B. Temperature dependence

Figures 7 and 8 report the temperature dependence of $G(\omega)$ computed from IN4 data measured with a wavelength of 1.22 Å and from IN6 data at 300K. It is worth mentioning that strong elastic scattering from the sample, via the instrumental resolution, and from the sample environment inevitably contributes to the inelastic signal and result in an intensity rise at low energies. This effect is enforced upon decreasing temperature as the inelastic signal is reduced by the Bose-Einstein population factor. For this reason, in these figures, IN4 data have been

suppressed below 5 meV. Even though Mo_3Sb_7 undergoes a spin gap formation concomitant with a cubic-to-tetragonal structural phase transition at 53 K, no significant changes are captured in the inelastic response of the compound. This observation is consistent with the small magnitude of the structural distortion as concluded from low temperature x-ray diffraction studies (Table I).^{13,14} In addition, no clear signature of spin excitations above and/or below T^* could be unraveled in the present measurements. Of course, this statement holds only within the accuracy of the performed experiments. The phase-space limit towards low- Q values (see Figure 2) and the strong elastic signal up to 5 meV might obscure dynamic fingerprints of a spin gap at low temperatures. Further investigations should therefore be carried out at lower Q values or with another technique such as neutron polarized experiments which might enable a separation of the magnetic and phonon contributions. As shown by the low-energy region of $G(\omega)$ obtained at IN4 using a wavelength of 1.8 Å (Figure 8), increasing temperature from 2 to 300 K leads to a progressive softening of the GDOS for both compounds. Such a temperature dependence can usually be understood within the quasiharmonic model which assumes that variations in phonon frequency originate from the thermal expansion.³⁰ In this context, the variation of the average phonon energy, $\langle E \rangle$, can be quantified through the relation $\gamma_G = -d \ln \langle E \rangle / d \ln V$ or equivalently, $\Delta E(T) / E_0 = -\gamma_G \Delta V(T) / V_0$ where γ_G is the Grüneisen parameter which can be expressed in terms of thermodynamic quantities³⁰

$$\gamma_G = \frac{3\alpha V B_T}{C_V} = \frac{3\alpha V B_S}{C_p} \quad (3)$$

where B_T and B_S are the isothermal and isentropic bulk moduli, respectively. A positive Grüneisen parameter, as typically observed in most materials, then results in a decrease of $\langle E \rangle$ with increasing temperature following the thermal expansion of the unit cell. To

determine whether or not the temperature dependence of the PDOS of both compounds can be adequately described by this model, the temperature dependence of the average phonon energy and of the three main peaks in $G(\omega)$ are plotted in Figure 9. The positions of these peaks, listed in Table V, were estimated by using both measured spectra at 1.22 and 1.80 Å in a similar fitting procedure as described above (Figure 9). The theoretical temperature dependence of $\langle E \rangle$ of Mo_3Sb_7 was calculated according to the quasiharmonic model using the thermal expansion coefficient inferred from neutron diffraction experiments and the Grüneisen parameter and bulk modulus derived from ultrasound velocity measurements.²¹ These experiments yielded $\gamma_G = 0.95$, $B = 72$ GPa and $\alpha = 25 \times 10^{-6}$ K⁻¹. Note that the experimental value of the bulk modulus is in very good agreement with the theoretical value of 73.6 GPa derived from the lattice dynamical calculations described in Section A. As a first approximation, the same values were used to determine the dependence of $\langle E \rangle$ on temperature for the Te substituted sample. As can be seen in Figure 9a, the parent compound shows a systematic decrease in energy of all the modes upon heating from 2 up to 300 K by a comparable amount. This gradual softening is however stronger in Mo_3Sb_7 than in the Te substituted sample (Figure 9b). The shift in energy induced by increasing the temperature affects the entire spectra as reflected by a similar amount of softening whatever the phonon mode is (Figure 9c). While the $\text{Mo}_3\text{Sb}_{5.4}\text{Te}_{1.6}$ compound follows the behaviour predicted by the quasiharmonic model, this theory fails to capture the temperature dependence of the phonon spectrum of Mo_3Sb_7 . Thus, the latter exhibits a higher degree of anharmonicity which falls beyond the quasiharmonic approximation. Another evidence of the anomalous behaviour of Mo_3Sb_7 is related to the contraction of the unit cell upon alloying with Te. At 300 K, this effect is expected to result in a stiffening of $\langle E \rangle$ of $\sim 0.12\%$ ($\Delta\langle E \rangle / E \sim 0.0012$) based on our experimental Grüneisen parameter. The observed stiffening of $\sim 7\%$ thus largely exceeds the

value expected for a pure volume contraction. These results are in agreement with low temperature heat capacity analyses revealing that the relation $C_p / T = \gamma + \beta T^2$, with βT^2 the lattice contribution, holds in a significantly broader temperature range in $\text{Mo}_3\text{Sb}_{5.4}\text{Te}_{1.6}$ with respect to Mo_3Sb_7 .¹⁶ This conclusion is also consistent with the thermal conductivity which follows the same trend i.e. lower values are observed in Mo_3Sb_7 than in $\text{Mo}_3\text{Sb}_{5.4}\text{Te}_{1.6}$.¹⁶ The stronger anharmonicity of Mo_3Sb_7 may also explain the discrepancy between the Debye temperatures derived from low-temperature specific heat and INS measurements (see Table II).

IV. Discussion

Non-harmonic effects in solids are usually related to phonon-phonon interactions or to interactions of phonons with electronic excitations.³⁰ The presence of magnetic dimers in Mo_3Sb_7 and their absence in $\text{Mo}_3\text{Sb}_{5.4}\text{Te}_{1.6}$ raises the question whether a strong interplay between phonons and dimers may be responsible for the strong phonon softening in Mo_3Sb_7 . As already mentioned, it has been suggested that strong phonons-dimers interactions are responsible for the unusual thermal transport in both Mo_3Sb_7 and in the ternary $\text{Mo}_3\text{Sb}_{7-x}\text{Te}_x$ and $\text{Mo}_{3-x}\text{Ru}_x\text{Sb}_7$ systems.^{15,16,18} An increase in the Te and Ru content results in a progressive suppression of the magnetic interactions as revealed by magnetic susceptibility data which in turn, leads to an increase in the thermal conductivity values. The strong anharmonicity observed in Mo_3Sb_7 and its absence in $\text{Mo}_3\text{Sb}_{5.4}\text{Te}_{1.6}$ might therefore corroborate this scenario.

Alternatively, softer phonons than expected from a pure volume expansion can arise in materials whose Fermi level is located close to sharp features in the electronic DOS such as in Cr, Mo, Nb or in the V_3Si and V_3Ge superconductors. The electron-phonon interaction exhibited by these materials was found to substantially affect the phonon energies leading to

an excess phonon softening even at temperatures well above the Debye temperature.^{32,33} In particular, in the above-mentioned superconductors, the departure from the quasiharmonic model was correlated to the strength of the electron-phonon coupling which causes a stiffening of the PDOS upon increasing the temperature.³² Electronic band structure calculations carried out on Mo_3Sb_7 have shown that the Fermi level lies near sharp features suggested to be at the core of the nearly zero thermopower observed below ~ 25 K.^{12,15} Thus, the Mo_3Sb_7 compound shares some similarities with the aforementioned elements and alloys which might be the origin of the extra softening observed. Since the partial substitution of Sb by Te results in both a shift of the Fermi level towards the band gap and a lift of the sharp features, this could also explain the absence of a departure from the quasi-harmonic model in the Te substituted sample as well as the strong stiffening of the PDOS upon alloying.¹⁶

Since superconductivity and magnetism coexist in Mo_3Sb_7 and are progressively suppressed in $\text{Mo}_3\text{Sb}_{7-x}\text{Te}_x$ and $\text{Mo}_{3-x}\text{Ru}_x\text{Sb}_7$ with increasing x , both electronic properties might be at the heart of the observed behaviour. At low Te concentration, low temperature transport properties measurements have shown that the electron-phonon coupling is significantly decreased whereby destroying the superconductivity while the magnetic properties remain practically unperturbed.¹⁶ Thus, further experiments performed at small Te substitution levels should help to disentangle the role played by these interactions on phonons in Mo_3Sb_7 and in the ternary derivatives.

Conclusion

Temperature dependence of the generalized density of states $G(\omega)$ of Mo_3Sb_7 and $\text{Mo}_3\text{Sb}_{5.4}\text{Te}_{1.6}$ was measured by inelastic neutron scattering in the 2 – 300 K temperature range. The experimental $G(\omega)$ of Mo_3Sb_7 is in good agreement with the phonon density of

states derived by lattice dynamical calculations. Within the accuracy of the experiments, no magnetic excitations could be observed in the temperature range investigated. The structural transition concomitant to the spin gap formation does not result in marked differences of the measured spectra below and above the characteristic temperature T^* . The partial substitution of Sb by Te leads to a shift of the entire $G(\omega)$ towards higher energy consistent with the decrease of the unit cell volume. Upon cooling, the $G(\omega)$ of Mo_3Sb_7 revealed a strong softening which is more pronounced than expected from the volume thermal expansion within the quasi-harmonic approximation. Since substituting Sb by Te suppresses this strong softening as it suppresses the magnetic interactions, the interplay of phonons and antiferromagnetically coupled molybdenum dimers is conjectured to be the origin of the enhanced anharmonicity. This interplay may be as well made responsible for the anomalous thermal transport in those materials. To further probe the magnetic behaviour in Mo_3Sb_7 below T^* may require investigations on high-quality single crystal by phonon spectroscopy techniques and/or by neutron polarized experiments.

Acknowledgement

C.C. greatly thanks M. Amiet and P. Maigné, and financial support of DGA (Délégation Générale pour l'Armement, Ministry of Defence, France) and of the European Network of Excellence CMA (Complex Metallic Alloys).

References

- ¹M. M. Koza, M. R. Johnson, R. Viennois, H. Mutka, L. Girard, and D. Ravot, *Nature Mat.*, **7**, 805 (2008).
- ²M. D. Lumsden, A. D. Christianson, E. A. Goremychkin, S. E. Nagler, H. A. Mook, M. B. Stone, D. L. Abernathy, T. Guidi, G. J. MacDougall, C. de la Cruz, A. S. Sefat, M. A. McGuire, B. C. Sales, and D. Mandrus, *Nature Phys.*, **6**, 182 (2010).
- ³A. D. Christianson, E. A. Goremychkin, R. Osborn, S. Rosenkranz, M. D. Lumsden, C. D. Malliakas, I. S. Todorov, H. Claus, D. Y. Chung, M. G. Kanatzidis, R. I. Bewley, and T. Guidi, *Nature*, **456**, 930 (2008).
- ⁴R. Coldea, D. A. Tennant, E. M. Wheeler, E. Wawrzynska, D. Prabhakaran, M. Telling, K. Habicht, P. Smeibidl, and K. Kiefer, *Science*, **327**, 177 (2010).
- ⁵Z. Bukowski, D. Badurski, J. Stepien-Damm and R. Troc, *Sol. Stat. Comm.*, **123**, 283 (2002).
- ⁶V.H. Tran, W. Müller, and Z. Bukowski, *Phys. Rev. Lett*, **100**, 137004 (2008).

- ⁷C. Candolfi, B. Lenoir, A. Dauscher, J. Hejtmanek, E. Santava, and J. Tobola, *Phys. Rev. B*, **77**, 092509 (2008).
- ⁸R. Khasanov, P.W. Klamut, A. Shengelaya, Z. Bukowski, I.M. Savic, C. Baines, and H. Keller, *Phys. Rev. B*, **78**, 014502 (2008).
- ⁹V. H. Tran, D. Hillier, D. T. Adroja, and Z. Bukowski, *Phys. Rev. B*, **78**, 172505 (2008).
- ¹⁰R. Khasanov, P.W. Klamut, A. Shengelaya, I.M. Savic, C. Baines, and H. Keller, *Phys. Rev. B*, **82**, 016501 (2010); V. H. Tran, D. Hillier and D. T. Adroja, *Phys. Rev. B*, **82**, 016502 (2010).
- ¹¹V. H. Tran, W. Miiller, and Z. Bukowski, *Acta Mater.*, **56**, 5694 (2008).
- ¹²B. Wiendlocha, J. Tobola, M. Sternik, S. Kaprzyk, K. Parlinski, and A. M. Oles, *Phys. Rev. B*, **78**, 060507(R) (2008).
- ¹³T. Koyama, H. Yamashita, Y. Takahashi, T. Kohara, I. Watanabe, Y. Tabata, and H. Nakamura, *Phys. Rev. Lett.*, **101**, 126404 (2008).
- ¹⁴T. Koyama, H. Yamashita, T. Kohara, Y. Tabata, and H. Nakamura, *Mat. Res. Bull.*, **44**, 1132 (2009).
- ¹⁵C. Candolfi, B. Lenoir, A. Dauscher, E. Guilmeau, J. Hejtmanek, J. Tobola, B. Wiendlocha, and S. Kaprzyk, *Phys. Rev. B*, **79**, 035114 (2009).
- ¹⁶C. Candolfi, B. Lenoir, A. Dauscher, J. Tobola, and J. Hejtmanek, *Phys. Rev. B*, **79**, 235108 (2009).
- ¹⁷C. Candolfi, B. Lenoir, C. Chubilleau, A. Dauscher, and E. Guilmeau, *J. Phys. C: Condens. Matter*, **22**, 025801 (2010).
- ¹⁸C. Candolfi, B. Lenoir, A. Dauscher, J. Hejtmanek, and J. Tobola, *Phys. Rev. B*, **80**, 155127 (2009).
- ¹⁹C. Candolfi, B. Lenoir, J. Leszczynski, A. Dauscher, and E. Guilmeau, *J. Appl. Phys.*, **105**, 083701 (2009).

- ²⁰V. H. Tran, D. Hillier, D. T. Adroja, Z. Bukowski, and W. Müller, *J. Phys. C: Condens. Matter*, **21**, 485701 (2009).
- ²¹C. Candolfi, B. Lenoir, A. Dauscher, J. Tobola, S. J. Clarke, and R. I. Smith, *Chem. Mat.*, **20**, 6556 (2008).
- ²²M. M. Koza, *Phys. Rev. B*, **78**, 064303 (2008).
- ²³S. Rols, H. Jobic, and H. Schober, *C. R. Phys.* **8**, 777 (2007).
- ²⁴S. Lovesey, *Theory of Neutron Scattering from Condensed Matter* (Oxford Science, Oxford, 1984).
- ²⁵G. Squires, *Introduction to the Theory of Thermal Neutron Scattering* (Dover, Mineola, NY, 1996).
- ²⁶H. Mutka, M. M. Koza, M. R. Johnson, Z. Hiroi, J.-I. Yamaura and Y. Nagao, *Phys. Rev. B*, **78**, 104307 (2008).
- ²⁷K. Parlinski, Z.-Q. Li, and Y. Kawazoe, *Phys. Rev. Lett.* **78**, 4063 (1997); K. Parlinski, Computer code PHONON, Cracow, 2008.
- ²⁸G. Grimvall, *Thermophysical Properties of Materials* (North-Holland, Amsterdam, 1999).
- ²⁹C. Candolfi, B. Lenoir, J. Leszczynski, A. Dauscher, J. Tobola, S. J. Clarke, R. I. Smith, *Inorg. Chem.*, **48**, 5216 (2009).
- ³⁰B. Fultz, *Prog. Mater. Sci.*, **55**, 247 (2010).
- ³¹C. Candolfi, B. Lenoir, A. Dauscher, C. Bellouard, J. Hejtmanek, E. Santava, and J. Tobola, *Phys. Rev. Lett.*, **99**, 037006 (2007).
- ³²O. Delaire, M. S. Lucas, J. A. Munoz, M. Kresch and B. Fultz, *Phys. Rev. Lett.*, **101**, 105504 (2008).
- ³³O. Delaire, M. Kresch, J. A. Munoz, M. S. Lucas, J. Y. Y. Lin, and B. Fultz, *Phys. Rev. B*, **77**, 214112 (2008) and references therein.

Tables

Table I. Lattice parameters, a , of the Mo_3Sb_7 and $\text{Mo}_3\text{Sb}_{5.4}\text{Te}_{1.6}$ compounds. The possible low-temperature crystal structure of Mo_3Sb_7 based on X-ray powder diffraction refinements is also given.

	Mo_3Sb_7	Mo_3Sb_7	$\text{Mo}_3\text{Sb}_{5.4}\text{Te}_{1.6}$
T (K)	298	10	298
Space group	$Im\bar{3}m$	$I4/m\bar{m}m$	$Im\bar{3}m$
a (Å)	9.5688	9.5611	9.5648
c (Å)	/	9.5388	/
Volume at 300 K (Å ³)	876.14	871.98	875.04

Table II. Debye temperature, θ_D , inferred from inelastic neutron scattering (INS) and low-

temperature specific heat analyses of Mo_3Sb_7 and $\text{Mo}_3\text{Sb}_{5.4}\text{Te}_{1.6}$. The values obtained via neutron diffraction and ultrasound velocity measurements for Mo_3Sb_7 are also given.

	Mo_3Sb_7	$\text{Mo}_3\text{Sb}_{5.4}\text{Te}_{1.6}$
INS	255	272
C_p	310	275
Neutron diffraction	300	/
Ultrasound velocity	285	/

Table III. Values of the on-side force constants (xx component) modified leading to the disappearance of the mode centred around 2 THz. The relative changes are given with respect to the (0 0) force constant which amounts to 122 990. The remaining 344 force-constant parameters are only changed by 0.0013 to 0.018 % which is within the numerical accuracy.

Atom 1	Atom 2	Distance (Å)	Force constant prior model (Ref. 12)	Force constant new model	Relative change (%)
Mo	Mo	0.0	122 990	123 204	0.174
Sb	Sb	0.0	80797	80797	0.755
Mo	Mo	3.045	-25472	-25686	0.174
Sb	Sb	3.408	-1373	-1930	0.689
Mo	Mo	4.664	5258	4707	0.164
Sb	Sb	4.820	-1771	-1484	0.682

Table IV. Coherent (σ_{coh}) and incoherent (σ_{inc}) neutron scattering cross sections given in barns, atomic mass and total scattering power ($\sigma_t / M = (\sigma_{coh} + \sigma_{inc}) / M$) of the Mo, Sb and

Te atoms. For comparison purposes, the data for hydrogen have been added.

Element	σ_{coh}	σ_{inc}	M	σ_t / M
H	1.76	80.26	1.01	82
Mo	5.67	0.040	95.94	0.059
Sb	3.90	0.007	121.76	0.032
Te	4.23	0.090	127.60	0.034

Table V. Temperature dependence of the three main peaks characterizing the lower part of the GDOS of Mo_3Sb_7 and $\text{Mo}_3\text{Sb}_{5.4}\text{Te}_{1.6}$ as inferred from IN4 data. Room temperature data obtained from IN6 experiments are also included.

Mo_3Sb_7					
2 K	8.80	11.45	13.23	15.28	18.95
70 K	8.71	11.47	13.33	15.26	18.81
220 K	8.44	11.51	12.96	15.05	18.81
300 K	8.41	11.27	12.83	14.88	18.64
$\text{Mo}_3\text{Sb}_{5.4}\text{Te}_{1.6}$					
2 K	9.33	12.02	14.68	18.54	20.60
70 K	9.36	12.07	14.66	18.45	20.55
220 K	9.29	11.98	14.74	18.40	20.38
300 K	9.16	11.95	14.38	18.26	20.57

Figure captions

Figure 1: (Color online) Generalized density of states $G(\omega)$ of Mo_3Sb_7 (blue open symbols) and $\text{Mo}_3\text{Sb}_{5.4}\text{Te}_{1.6}$ (red full symbols) at 300 K as derived from IN6 measurements.

Figure 2: $S(Q, \omega)$ maps of Mo_3Sb_7 recorded at IN6 at 300 K and IN4 at 220 K. For comparison purposes, IN4 intensity has been rescaled from 220 K to 300 K via the Bose-Einstein occupation number. Data have been collected with a wavelength of 4.14 Å and 1.8 Å at IN6 and IN4, respectively.

Figure 3: Phonon dispersion curves of Mo_3Sb_7 along high symmetry directions. Upper panel: results derived and discussed in Ref. 12. Lower panel: with introduction of a dispersion of the flat phonon mode in the N-H direction.

Figure 4: (Color online) Phonon density of states $Z(\omega)$ of Mo_3Sb_7 as obtained from ab initio lattice dynamics calculations. (a) Total $Z(\omega)$ as computed (dotted line) and convolved with a

Gaussian (red full line) reflecting the energy-dependent resolution of the IN6 spectrometer.
 (b) Partial $Z(\omega)$ of Mo (red dashed line), of Sb(1) (green dotted line) and Sb(2) (blue full line).

Figure 5: (Color online) (a) Theoretical (\circ) and experimental (\square) temperature dependence of the specific heat of Mo_3Sb_7 . The kink observed near 50 K corresponds to the spin gap formation. (b) Specific heat plotted as C_p/T^3 versus T to highlight the match between the theoretical and experimental data at low temperatures.

Figure 6: (Color online) Temperature dependence of the experimental specific heat $C_p(T)$ (\circ), the lattice contribution inferred from INS data (\square) along with the electronic contribution (Δ) and the magnetic contribution (\bullet) for Mo_3Sb_7 (a) and $\text{Mo}_3\text{Sb}_{5.4}\text{Te}_{1.6}$ (b).

Figure 7: (Color online) $G(\omega)$ at the different temperatures of 2, 100 and 300 K. Left, $G(\omega)$ of Mo_3Sb_7 , right, $G(\omega)$ of $\text{Mo}_3\text{Sb}_{5.4}\text{Te}_{1.6}$. IN4 data plotted as line style are taken with an incident wavelength of 1.2 Å. High resolution data taken at IN6 are plotted with full symbols, blue for Mo_3Sb_7 , and red for $\text{Mo}_3\text{Sb}_{5.4}\text{Te}_{1.6}$.

Figure 8: (Color online) Temperature dependence of $G(\omega)$ of the Mo_3Sb_7 and $\text{Mo}_3\text{Sb}_{5.4}\text{Te}_{1.6}$ compounds recorded at the different temperatures of 2, 70 and 220 K at IN4 with a wavelength of 1.8 Å. The red and blue spectra represent the measured $G(\omega)$ with IN6 of Mo_3Sb_7 and $\text{Mo}_3\text{Sb}_{5.4}\text{Te}_{1.6}$, respectively. The $G(\omega)$ intensities have been normalized to that of the IN6 data in the 8-21 meV energy range.

Figure 9: (Color online) Temperature dependence of the mean phonon energy $\langle E \rangle$ for the (a) Mo_3Sb_7 (\square) and (b) $\text{Mo}_3\text{Sb}_{5.4}\text{Te}_{1.6}$ (\circ) compounds. The black solid lines are guide to the eye while the dashed line stands for the theoretical temperature dependence following the quasi-harmonic model. Note that, at any given temperature, $\langle E \rangle$ was determined using data above 5 meV to avoid the contribution due to the strong elastic signal. Error bars are from experimental counting statistics. (c) Temperature dependence of the main phonon modes centered at $\hbar\omega \approx 8.4$ (\circ), 14.8 (\square) and 18.5 (Δ) meV for Mo_3Sb_7 (open symbols) and $\text{Mo}_3\text{Sb}_{5.4}\text{Te}_{1.6}$ (filled symbols).

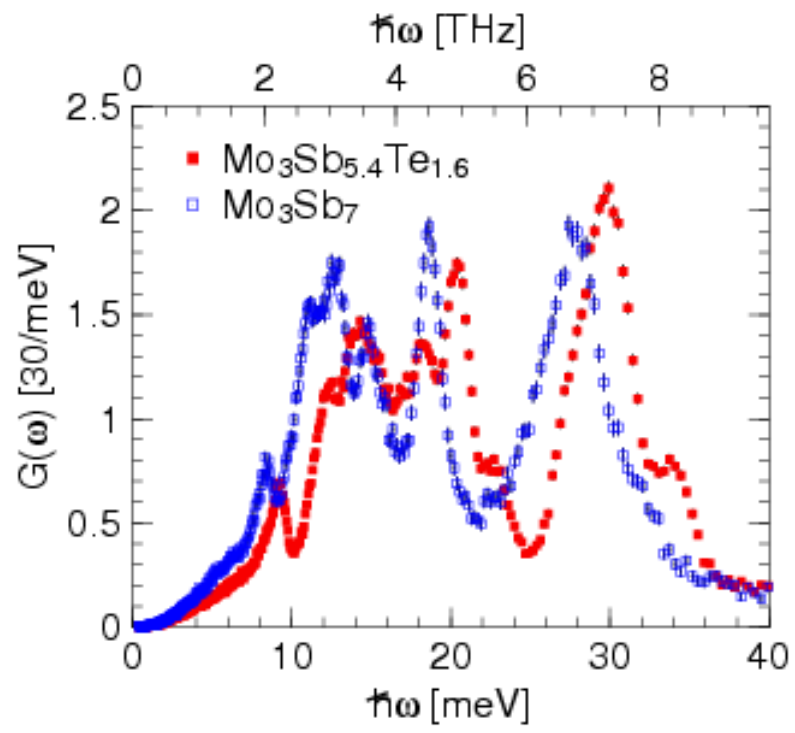


Figure 1

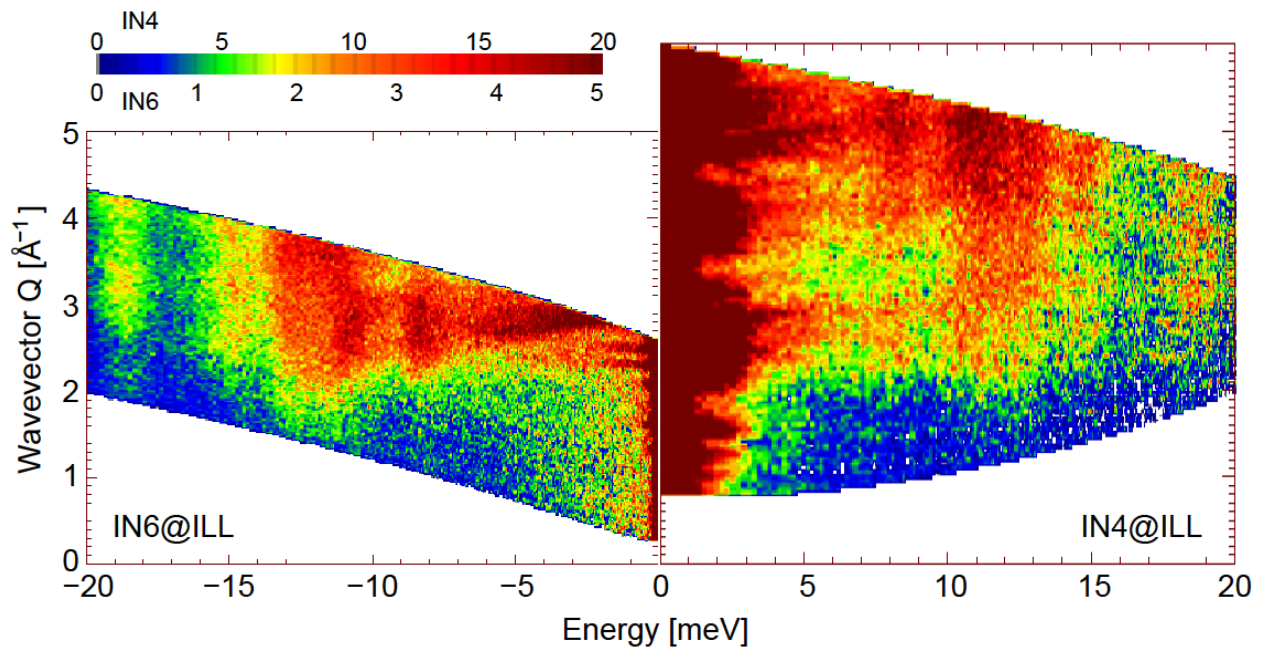


Figure 2

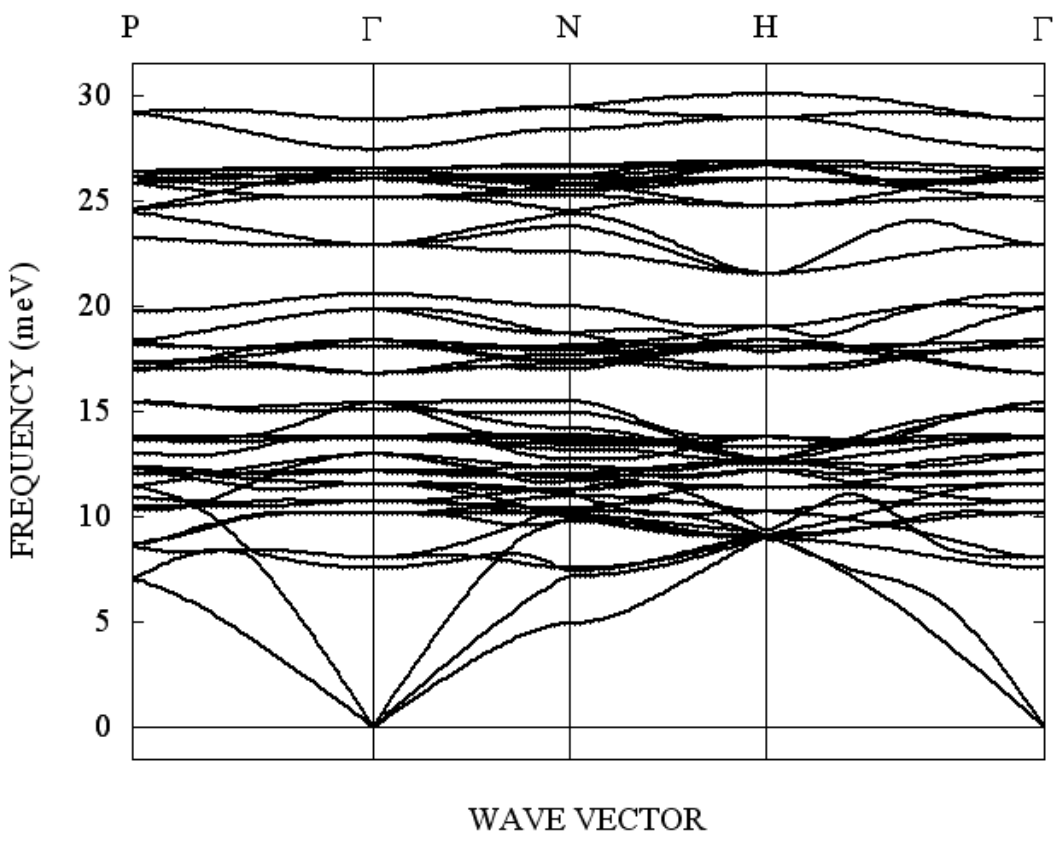
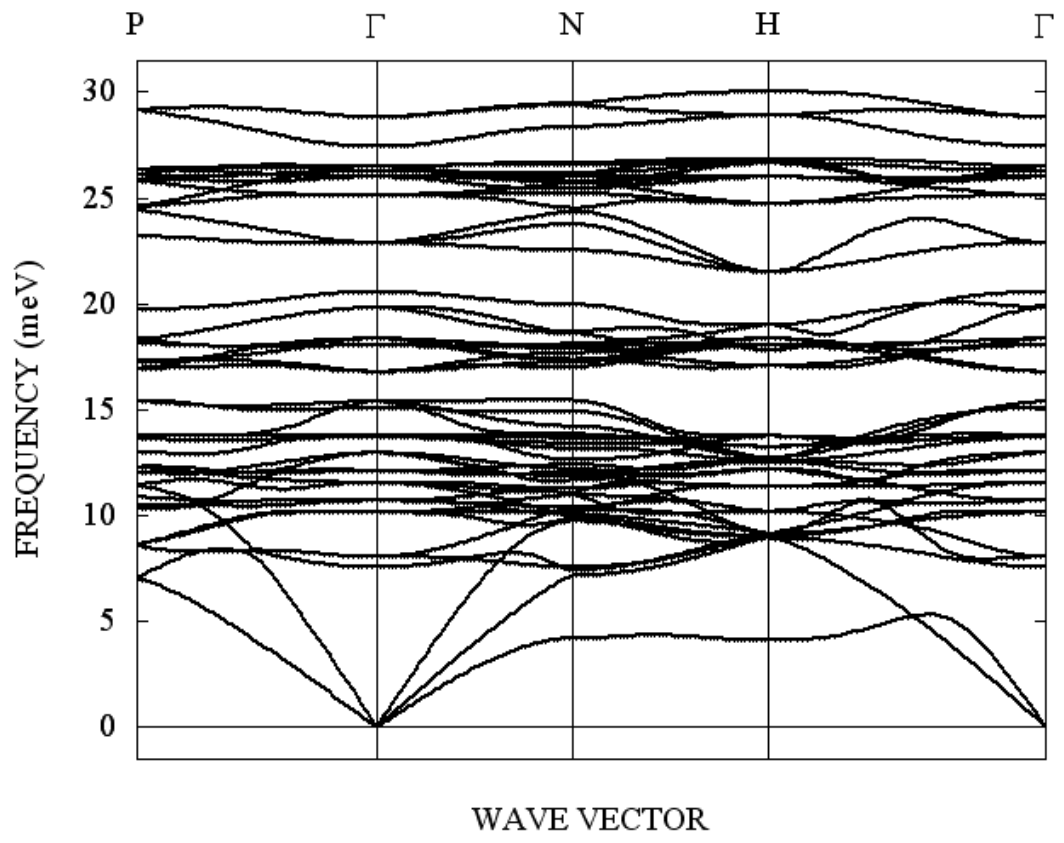


Figure 3

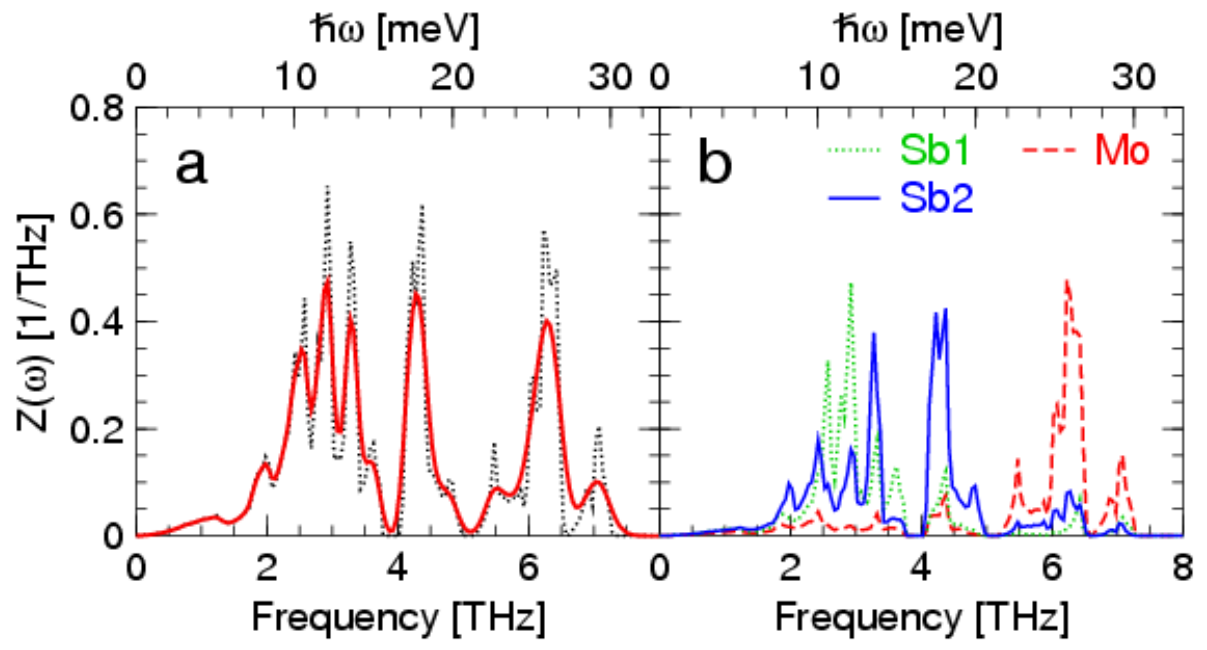


Figure 4

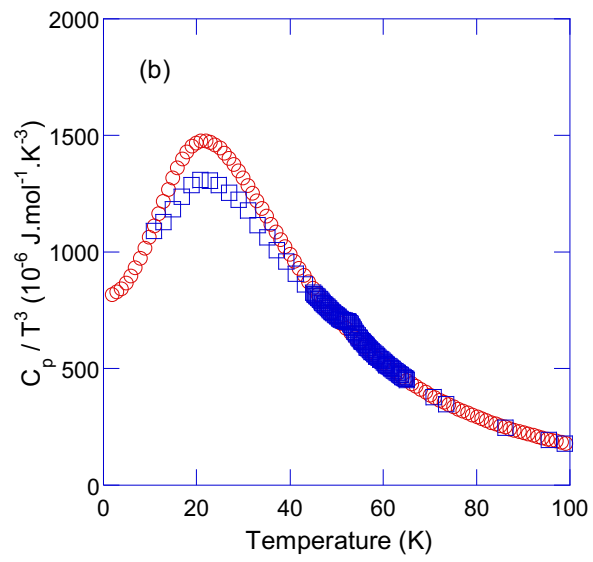
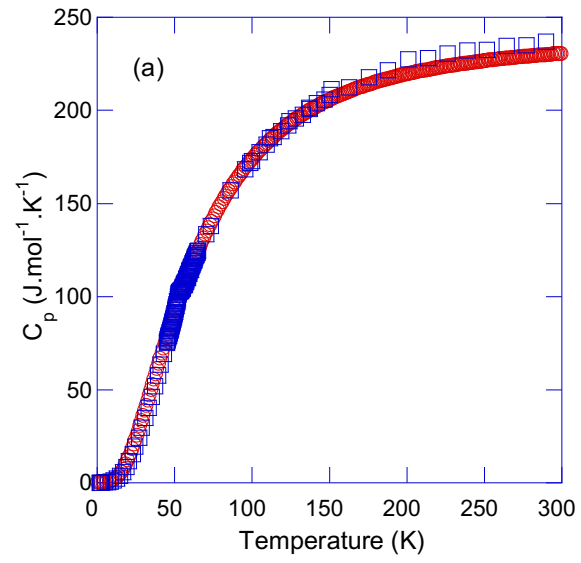


Figure 5

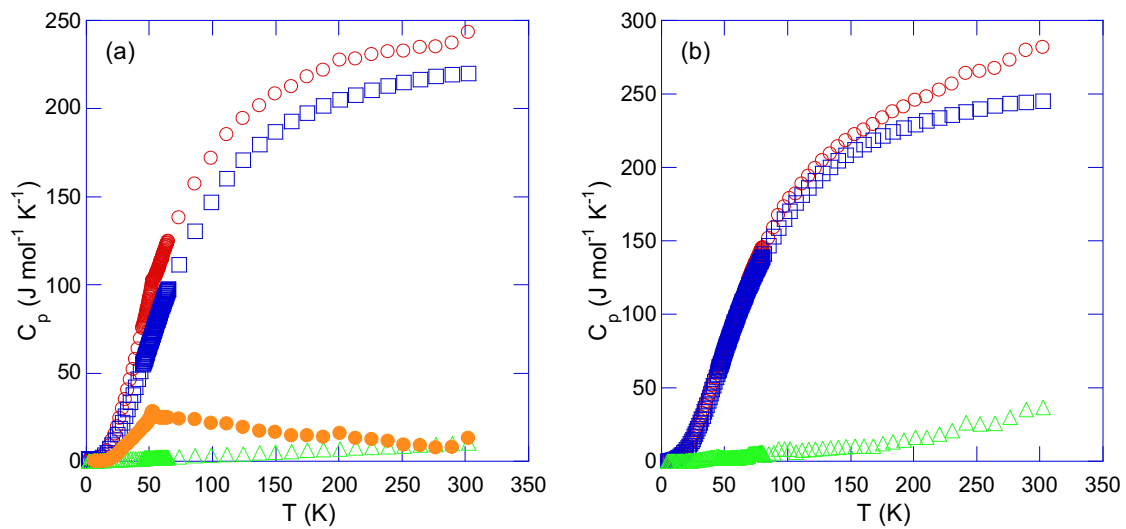


Figure 6

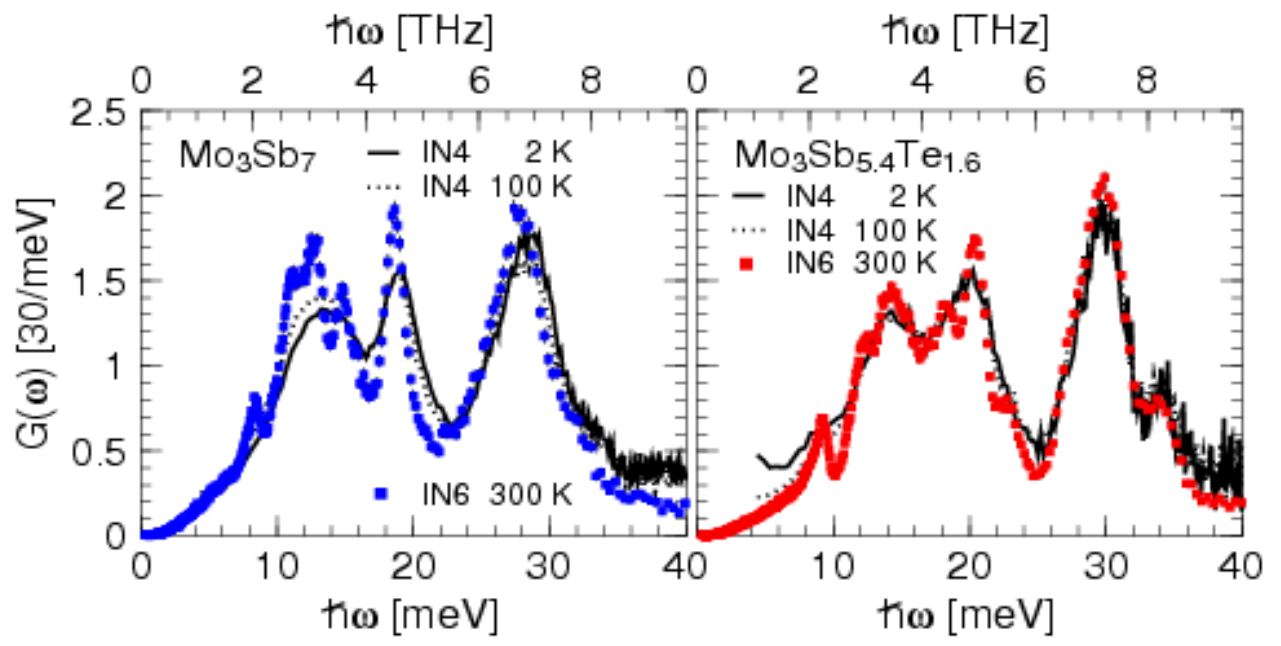


Figure 7

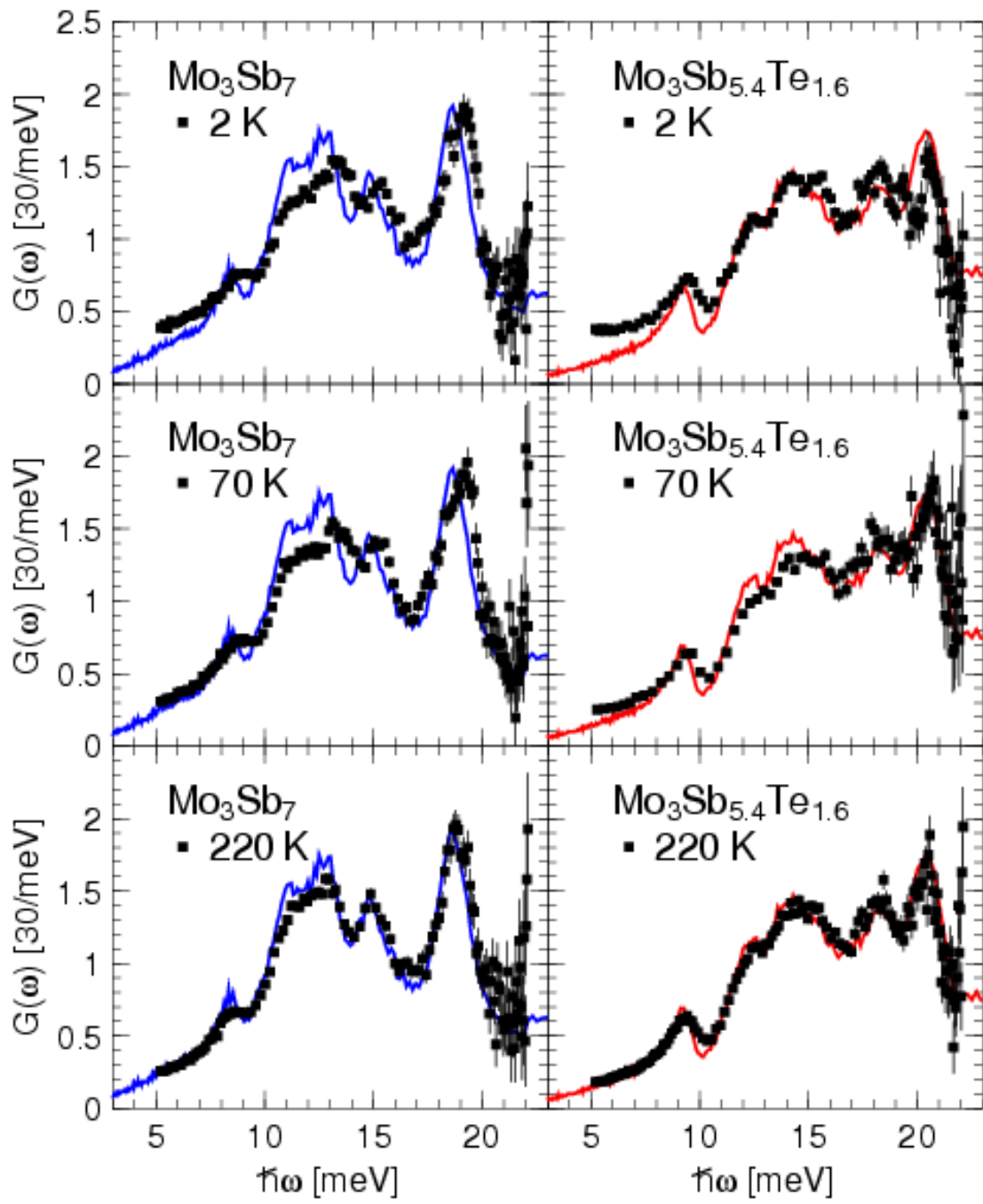


Figure 8

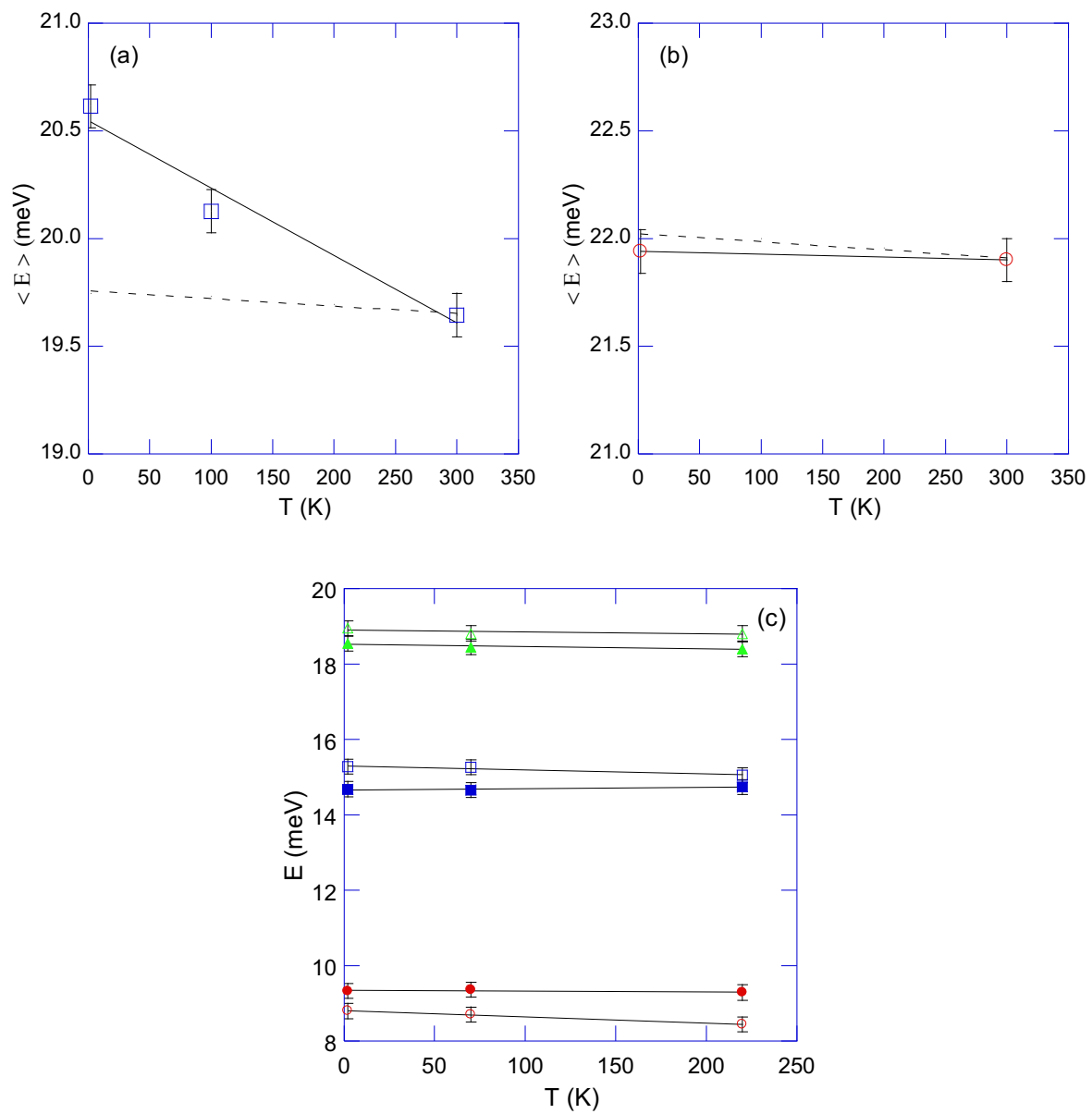


Figure 9